APL/JHU
S1R79U-035
DECEMBER 1979

# MULTI-YEAR SLANT PATH RAIN FADE STATISTICS AT 28.56 AND 19.04 GHz FOR WALLOPS ISLAND, VIRGINIA

by JULIUS GOLDHIRSH

SPACE DEPARTMENT
THE JOHNS HOPKINS UNIVERSITY ✱ APPLIED PHYSICS LABORATORY

APL/JHU
S1R79U-035
DECEMBER 1979

# MULTI-YEAR SLANT PATH RAIN FADE STATISTICS AT 28.56 AND 19.04 GHz FOR WALLOPS ISLAND, VIRGINIA

by JULIUS GOLDHIRSH

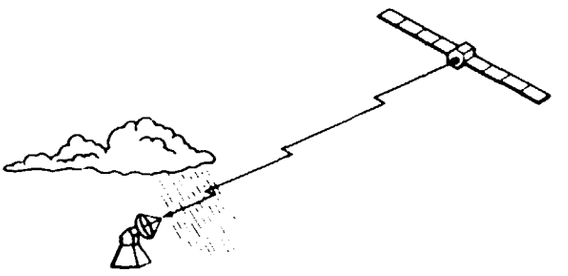

SPACE DEPARTMENT
THE JOHNS HOPKINS UNIVERSITY ■ APPLIED PHYSICS LABORATORY
Johns Hopkins Road, Laurel, Maryland 20810

Operating under Contract N00024 78 C 5384 with the Department of the Navy

## Table of Contents

Acknowledgements:

The author is grateful to Norman Gebo and Jack Howard at the NASA radar facility at Wallops Island, Virginia for assisting in the acquisition of the experimental data. Many thanks are also directed to Bert Musiani and Al Riley for their help in reducing the data. Much appreciation is also expressed to Karen Melvin for her efforts in typing this manuscript.

This work was performed under contract with NASA/Goddard Space Flight Center (NASA HDPR S50748A; Radar Prediction of Rain Attenuation for Earth Satellite Paths).

**Figures**

(square), and combined (triangular) monthly rainfalls. (Data obtained from the U.S. Navy and U.S. Weather Service for the Wallops Station).

Figure 15 Radar derived conditional fade distributions (solid points) compared with predicted levels (circled points). Radar data covers 17 hours of rainfall during 5 summer and 5 winter rain days.

Figure 16 Rain rate distributions for Regions $D_2$ and $D_3$ of global model (18) compared with measured distributions (combined years) for Wallops Island, Virginia.

Figure 17 Comparison of cumulative fade distributions for Wallops Island, Virginia with those predicted using the global model (18).

# Multiyear Slant-Path Rain Fade Statistics at 28.56 and 19.04 GHz for Wallops Island, Virginia


## Abstract

Multiyear rain fade statistics at 28.56 GHz and 19.04 GHz have been compiled for the region of Wallops Island, Virginia covering the time periods, 1 April 1977 - 31 March 1978, and 1 September 1978 - 31 August 1979. The 28.56 GHz attenuations were derived by monitoring the beacon signals from the COMSTAR geosynchronous satellite, $D_2$, during the first year, and satellite, $D_3$, during the second year. Although 19.04 GHz beacons exist aboard these satellites, statistics at this frequency were predicted using the 28 GHz fade data, the measured rain rate distribution, and effective path length concepts. The prediction method used was tested against radar derived fade distributions and excellent comparisons were noted. For example, the rms deviations between the predicted and test distributions were less than or equal to 0.2dB or 4% at 19.04 GHz. The average ratio between the 28.56 GHz and 19.04GHz fades were also derived for equal percentages of time resulting in a factor of 2.1 with a .05 standard deviation. These were compared with ratios derived from distributions measured at other locations and similar values near 2.0 were also observed.

Comparisons are made of yearly, monthly, and time of day fade statistics for the first, second and combined years.

Although considerable year to year variations in exceedance times exist for the monthly and time of day fade statistics, the overall fade distributions for the individual years showed relatively small differences. For example, comparing the second year fades relative to those of the first year at equal percentages of time, less than 20% rms deviation was found.

The year to year variations of rain rate distributions are also examined and show consistently small differences. The resultant fade distributions at 28.56 GHz and 19.04 GHz for Wallops Island, Virginia are compared with those arrived at using a prediction method which is a recent refinement of the C.C.I.R. global model, and rms deviations of less than 14% and 9% were noted at the respective frequencies.

## 1.0 Introduction

As future earth-satellite communications systems are being planned at frequencies above 10 GHz, the designers of such systems desire a knowledge of rain fade statistics for establishing link transmitter and receiver parameter requirements. In particular, they are interested in fade statistics established from meaningful data base; namely those calculated over a multiyear data period (1). They are also interested in the year to year variations of these statistics for purposes of establishing margins of uncertainties in their design criteria.

In this report we describe fade statistics derived from the monitoring of a 28.56 GHz beacon signal emanating from the COMSTAR geosynchronous satellite (2) over two non-contiguous years. These

data were acquired at the SPANDAR site at the NASA facility at Wallops Island, Virginia (37° 51' 16.8" N. latitude, 75° 30' 48.4" W. longitude), approximately 180 km S.E. of Washington, D. C., off the mid-Atlantic coast.

The results associated with the first year's data base (1 April 1977 - 31 March 1978) were previously described by Goldhirsh (3). We examine here the multiyear variations associated with the first and second year's data base (1 September 1978-31 August 1979), as well as the combined years results. Specifically, the yearly variations of the yearly, monthly, and time of day fade distributions as well as the yearly variations of the rain rate distributions are presented.

Sources at 19.04 GHz were also on board the COMSTAR satellites. As no receiver was available at this second frequency, the corresponding fade statistics were predicted. The prediction method used is tested against radar derived fade distributions at 28.56 and 19.04 GHz. Fade ratios of the 28 to 19 GHz levels are also examined at equal exceedance times and the average ratio is compared with those derived from the results of other investigators.

## 2.0 Experimental Aspects

### 2.1 General

As the details of the experimental system have, for the most part, been previously described (4), the following represents only a brief review. In addition, a description of some modifications are given.

The general experimental configuration at Wallops Island, Virginia is depicted in Fig. 1. During the first year period, the receiving antenna pointed in the direction of satellite $D_2$ (95° W longitude) with an azimuth and elevation of 210.0° and 41.6°, respectively. During the second year, the receiving antenna pointed towards the satellite, $D_3$ (87° W longitude) with an azimuth and elevation of 198.3° and 44.5°, respectively. The switch to the second satellite was a result of the beacon turnoff on $D_2$.

A phase lock loop receiving system (beamwidth = 0.4° and dynamic range ≈ 30dB) monitors the 28.56 GHz beacon signal continuously. During the second year period, a Faraday rotator switch had been located at the receiver antenna feed and cross polarized signal levels at 28.56 GHz were also sampled continuously. The cross polarized signals are being monitored to study the influence of high altitude ice crystal depolarizations which may occur during periods of little or no rainfall (5). This type of cross polarization is presently being reduced and analyzed and will be considered in a later report. Located nearby (1.57 m away) is a high resolution S Band radar which measures the rain reflectivity along the earth-satellite path for purposes of testing radar methods for estimating slant path rain attenuation (4). The radar which has a frequency of 2.84 GHz, peak power of $10^6$ watts and pulsewidth of 1 μsec, monitors the rain reflectivities at contiguous pulse volumes with a range resolution of 150 m. The results pertaining to the radar estimation of slant path attenuation have been previously described (4) and for the most part is not considered here.

| TYPE | SATELLITE LONG. | WI RECEIVER AZ | WI RECEIVER EL |
|---|---|---|---|
| $D_1$ | 128° W | 244.8° | 20.6° |
| $D_2$ | 95° W | 210.0° | 41.6° |
| $D_3$ | 87° W | 198.3° | 44.5° |

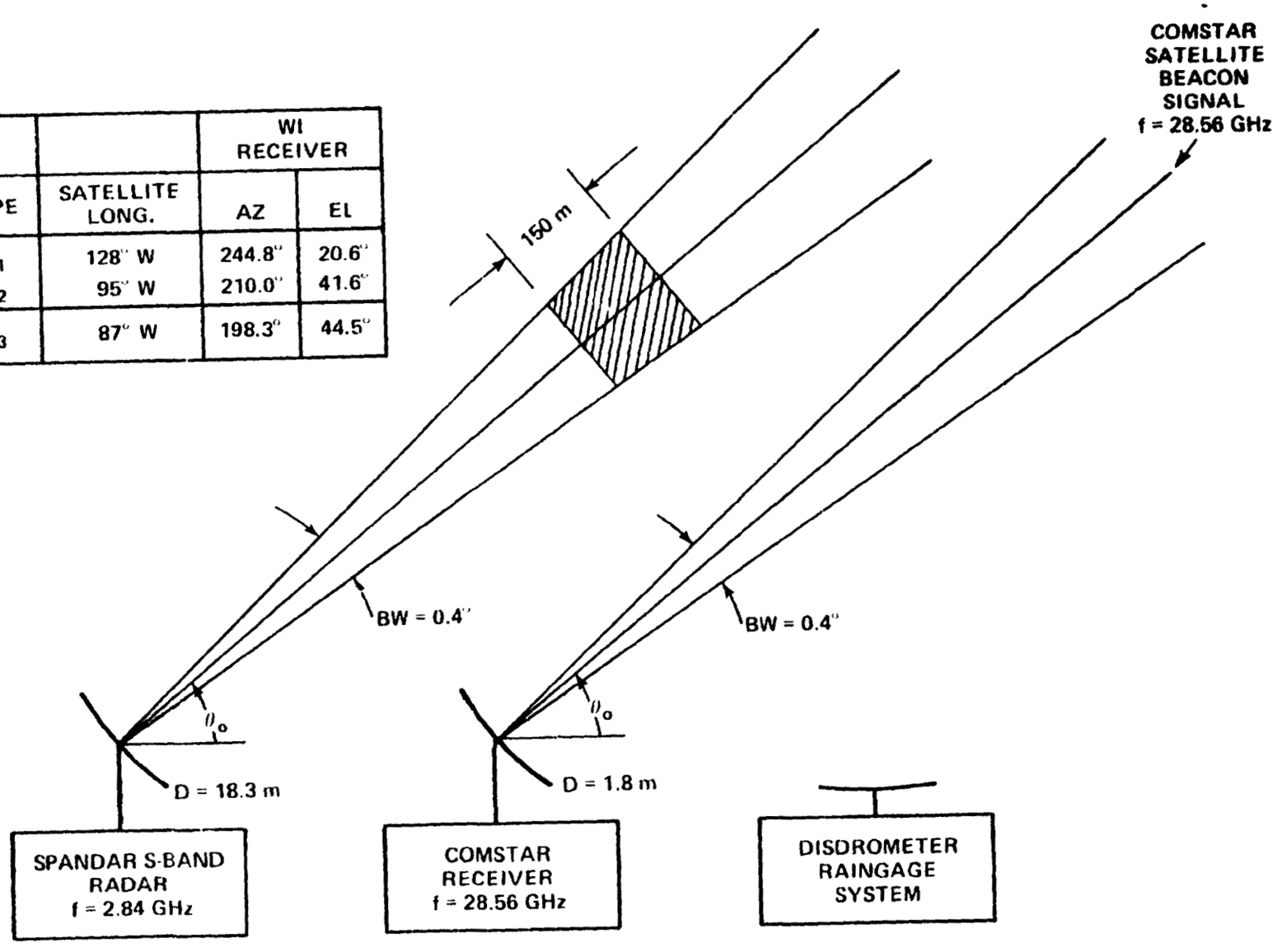


Figure 1. Experimental configuration at Wallops Island, Virginia.

Also located nearby (within 10 m away) is a disdrometer-raingage system which measures drop size spectra and rain rate, respectively (6). These measurements are used as inputs for the radar estimation methods of slant path attenuation. They are also employed for the estimation of the cumulative fade distribution at 19.04 GHz as described in Section 5.

## 2.2 Measurement and Recording Systems

Because many different measurements of data are simultaneously made, a minicomputer system was placed on-line during the second year period to efficiently handle and record these data. A block diagram describing the overall measurement and recording system is depicted in Fig. 2.

The incoming co-polarized signal passes through a Faraday switch, is down-converted in the front end unit and the I.F. (1.05 GHz) passes to a phase locked loop receiver. The receiver output (0 to 5 volts) feeds into an A/D unit-switching interface which injects the digitized receiver levels into an on-line HP 9825 minicomputer where it is sampled and recorded on magnetic disk. The switching interface also periodically transmits a current pulse to the Faraday switch which enables the cross polarized signal to pass into the receiver with negligible insertion loss while isolating the co-polarized signal (isolation being approximately 25 dB). Both co and cross-polarized signal levels are recorded on magnetic disk at a sampling rate of once per two seconds.

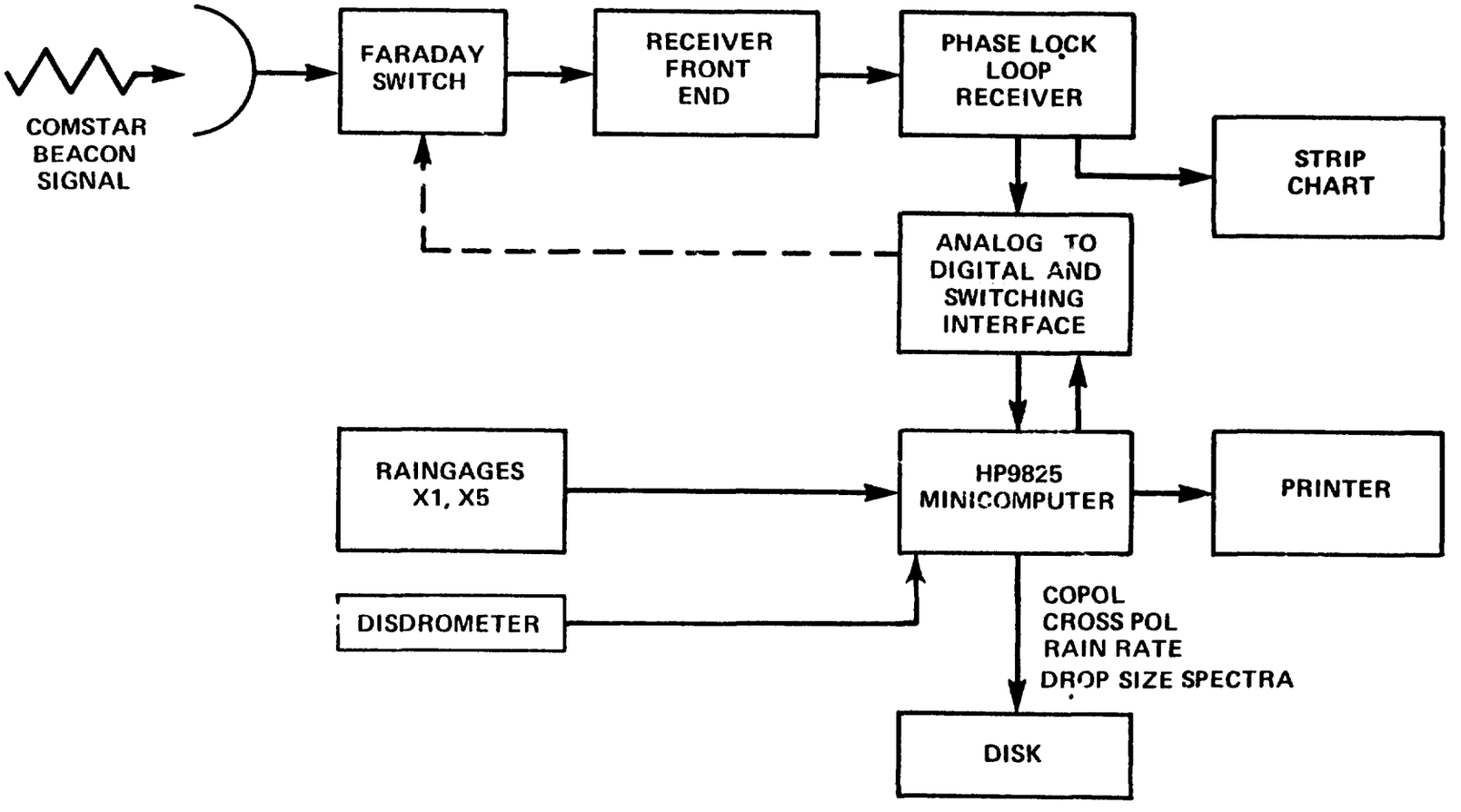


Figure 2. Simplified block diagram of system for monitoring co- and cross-polarization as well as simultaneous rain rates and disdrometer data.

The disdrometer data are also simultaneously monitored and recorded on magnetic disk (7). In addition, rain rates from two tipping bucket raingages, one with an enlarged funnel for improving the time resolution of smaller rain rates, are recorded on the magnetic disk. Time is also recorded periodically from an internal clock in the minicomputer. Receiver data may be recorded continuously for a period of 65 hours on each disk side. Receiver system calibrations are performed by injected 28.56 GHz signal levels through the front end and these are also recorded on a disk and are later recalled for reduction and analysis of the data.

## 3.0 Cumulative Fade Distributions

### 3.1 Yearly and Combined Years Distribution

In Fig. 3 are given the fade distributions for the first, second, and combined years data bases. The fades range from 3 to 28 dB and the exceedance times range approximately from 1% (87.6 hours) to .04% (3.5 hours). Above 25 dB, the fade statistics appear noisy (exceedance times smaller than 5 hours). Although the two yearly distributions are close to one another, the second year's exceedance times are somewhat larger than the first up to 25 dB. The average ratio of percentages down to 25 dB is 1.20 (average of larger percentages divided by smaller ones) and the rms deviation between the two yearly distributions is 2 dB or 18% relative to the first year's fade levels.

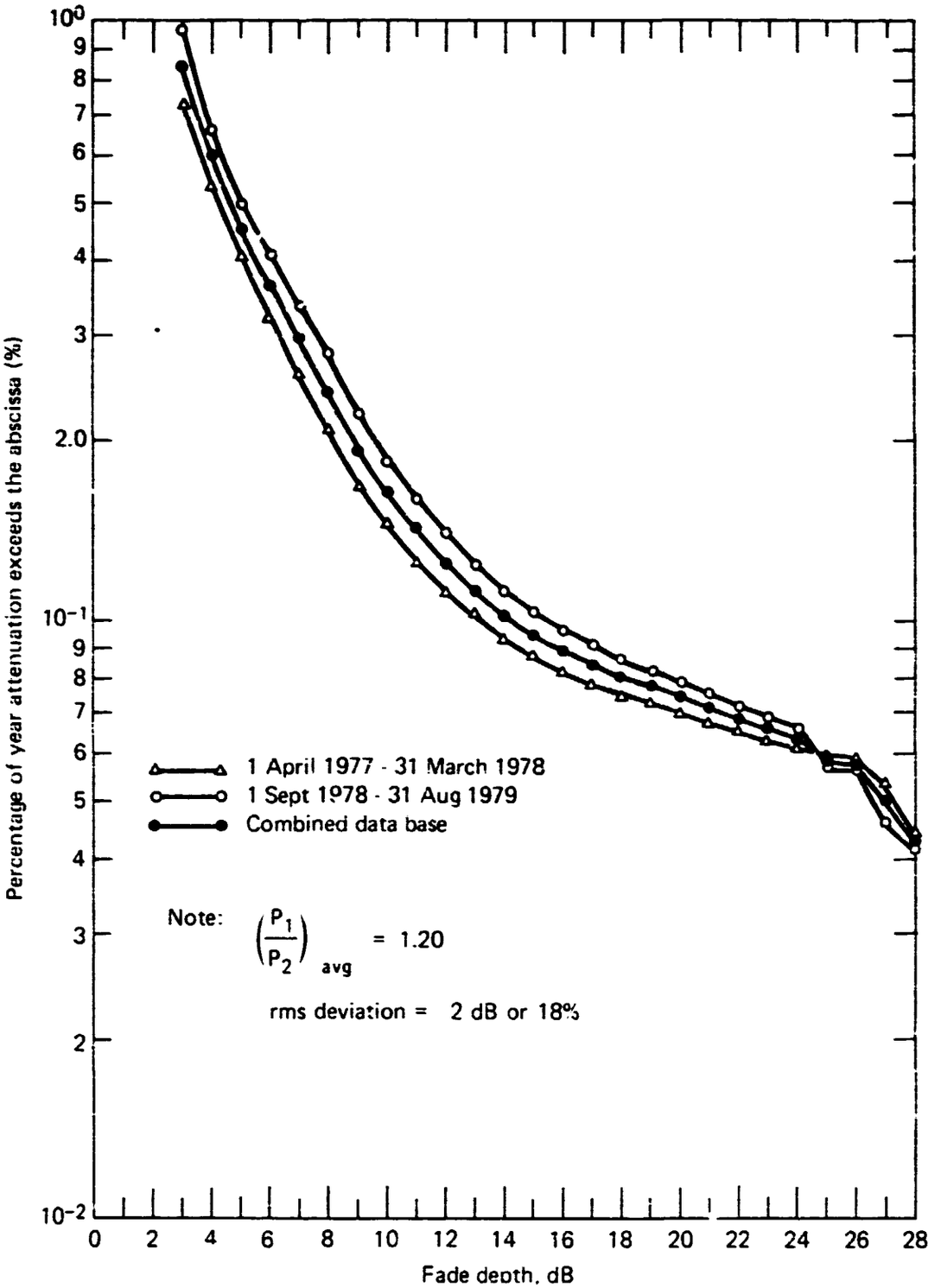


Figure 3. Cumulative fade distributions for 1st, 2nd, and combined years.

### 3.2 Comparison of 28.56 and 19.04 GHz Fade Distributions

In Fig. 4 are plotted both the 28.56 GHz measured distribution (combined years) as well as the estimated 19.04 GHz one. As mentioned, the method by which the 19.04 GHz distribution is calculated is described in Section 5. We note the lower frequency distribution ranges in fades between 1.3 to 12.6 dB over the same probability interval that the 28.56 GHz distribution ranges in fades between 3 and 25 dB. The average ratio of the 28.56 GHz fades to the 19.04 GHz fades calculated over a number of fixed probability levels was found to be 2.12 with a standard deviation of 0.05 (see Table 1). The results of Goldhirsh in Table 1 were calculated by the following two methods: (1) from the measured and estimated distributions at 28.56 and 19.04 GHz, respectively, over the two year period, and (2) by considering radar derived fade distributions at 28.56 and 19.04 GHz (as described in Section 5).

In Table 1 are also given similar ratios calculated from the results of other investigators for the same fade interval. The similarity of the ratio among the various investigator attests to the relative invariance of this ratio with drop size distribution (3). It is interesting to note that the calculated ratio is similar to that obtained by Drufuca (8) for the range 11.2 to 18.7 GHz; namely,

$$\frac{A_2}{A_1} = \left(\frac{f_2}{f_1}\right)^{1.72} \qquad (1)$$

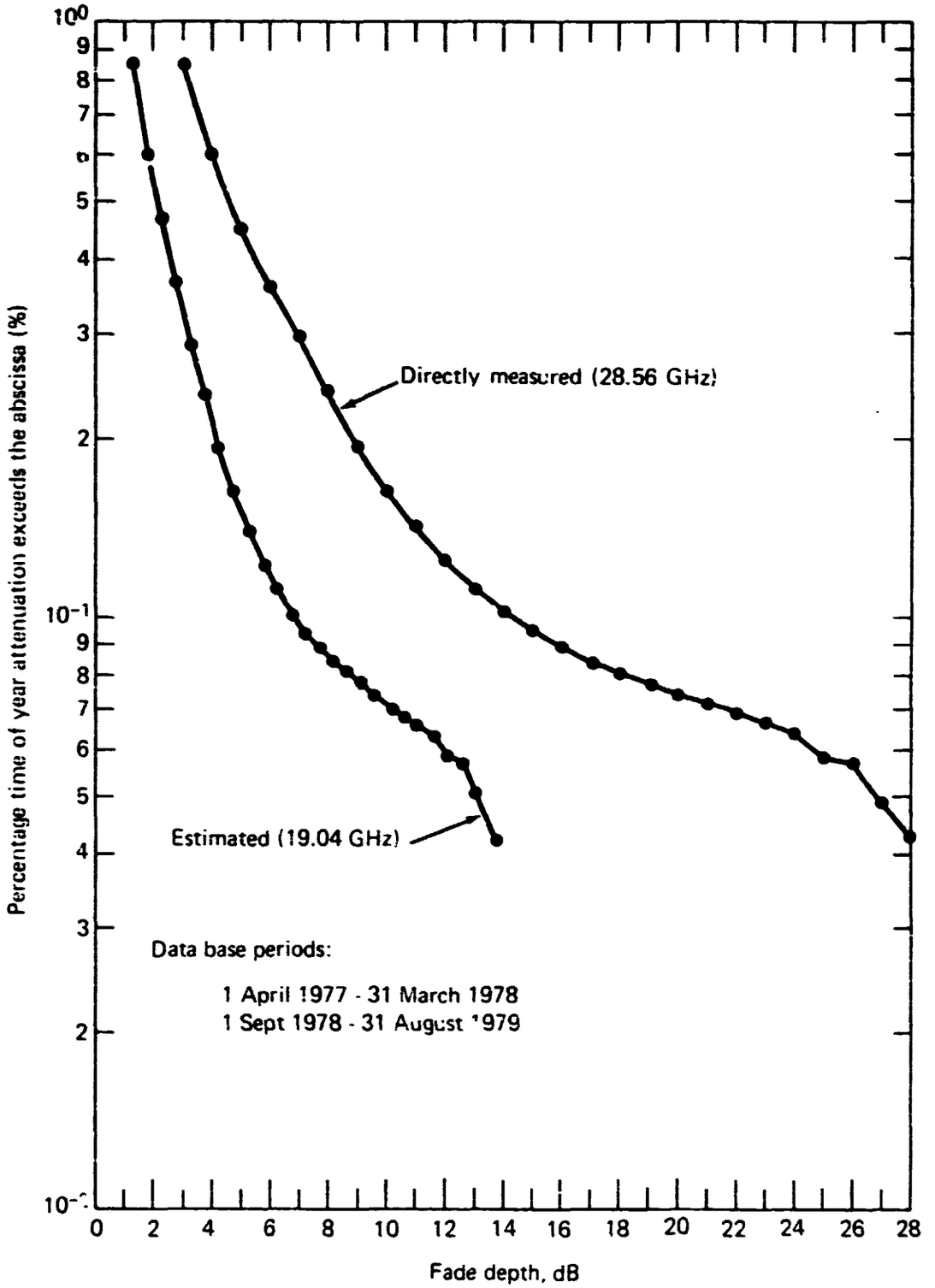


Figure 4. Comparison of cumulative distributions at 28.56 GHz (measured) and 19.04 GHz (estimated) over combined years.

Table 1 Ratios of $A_{28}/A_{19}$ as arrived at from results of various investigators over the same fade range ( 3 to 25 dB).

| Investigator | $(A_{28}/A_{19})_{avg}$ | S.D. | Location and Period |
|---|---|---|---|
| Harris and Hyde ( 9) | 1.92 | .09 | Clarksburg, Md. 6/76 to 1/77 |
| Bergmann (10) | 1.94 | .12 | Palmeto, Georgia 6/77 to 7/77 |
| Cox et al (11) | 2.18 | .07 | Crawford Hill, N.J. 5/77 to 5/78 |
| Goldhirsh measured 28.56 GHz estimated 19.04 GHz | 2.12 | .05 | Wallops Island 4/77-3/78 9/78-8/79 |
| Goldhirsh (radar data base) | 2.08 | .13 | Wallops Island summer 77 fall winter 78-79 |
| C. Bostion (Private Communication) December 10, 1979 | 2.17 | 0.66 | Blacksburg, Va. 1977 - 1979 (14 months, intermittent) |

where $A_2$ and $A_1$ are the fades at the respective frequencies, $f_1$ and $f_2$, for any given probability level. We observe that $A_2/A_1$ = 2.01 for the frequencies of 28.56 and 19.04 GHz, respectively.

### 3.3 Approximation to the Log Normal Distribution

In Fig. 5 are plotted the overall 28.56 and 19.04 GHz data points for the cumulative distribution on a log-normal scale; the ordinate and abscissa having Gaussian and logarithmic scales, respectively. The solid and dashed straight lines represent fitted log-normal distributions down to .08% and .05%, respectively (17 and 27 dB at 28.56 GHz). We note from the table in Fig. 5 that the data points for the former and latter cases for both frequencies deviate from their log normal estimates by less than 5% and 12% (peak) and 3% and 7% (rms), respectively.

These results are consistent with the contention of Lin (12) that, because the rain attenuation at any instant of time is multiplicatively affected by a large number of random time varying parameters of the environment, the central limit theorem applied to this characteristic leads to the lognormal distribution of the rain attenuation. It is shown in Section 4 that the rain rate distribution also gives an excellent lognormal fit; probably for similar reasons (Fig. 13).

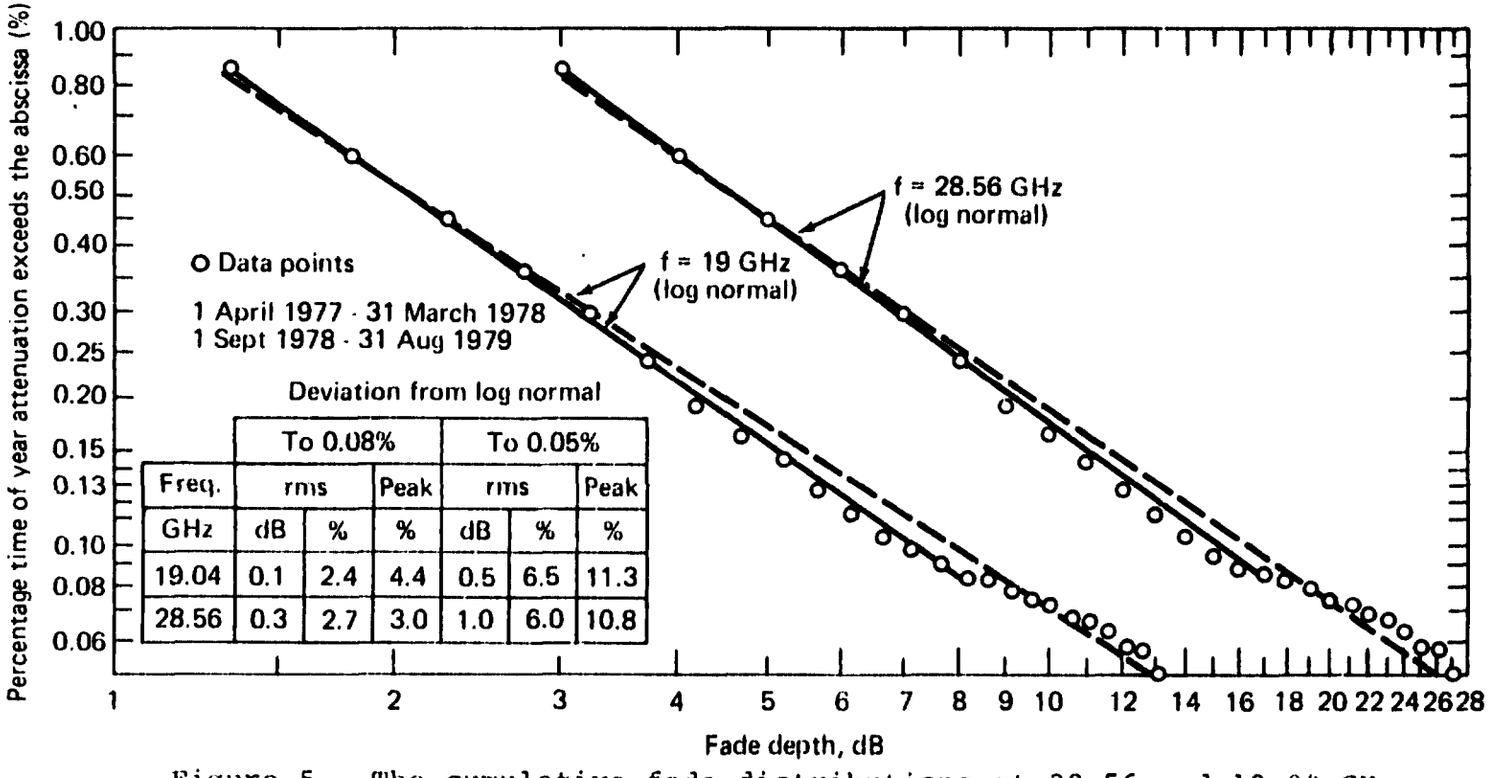


Figure 5. The cumulative fade distributions at 28.56 and 19.04 GHz plotted against log normal scales. The solid and dashed curves (straight lines) are fitted log normal distributions down to .08% and .05%, respectively.

## 3.4 Monthly Statistics

In Figs. 6-8 are plotted the monthly fade distribution for 28.56 GHz (combined data base) where the ordinate represents the percentage of the month the attenuation exceeds the abscissa. For 10 dB and greater, August is observed to have the largest exceedance times and hence represents the "worst" month for all fades greater than 10 dB. As matter of fact, upon superimposing all the distributions on a single page, we note that three groupings of distributions exist. The largest exceedance times occur from May through August, intermediate times occur during October, December, January and March, and minimum levels exist in February, April and September.

The year to year variations for the monthly fades are depicted in the histogram in Fig. 9; the vertical scale representing the percentage of time of month given threshold levels of fade, $A_q$, are exceeded. The threshold levels are 5dB (white), 15dB (cross hatch to right) and 25dB (cross hatch to left). The abscissa represents the corresponding month of the year where the numbers, 1, 2 and 3 denote the results corresponding to the first, second, and combined years, respectively. One may notice from examining an overview of the entire histogram that a general enhancement of the exceedance times exist from May through August at the higher fades. As a matter of fact, at a 15dB threshold level, May through August have exceedance times for the combined years which are approximately more than double those of the other 8 months.

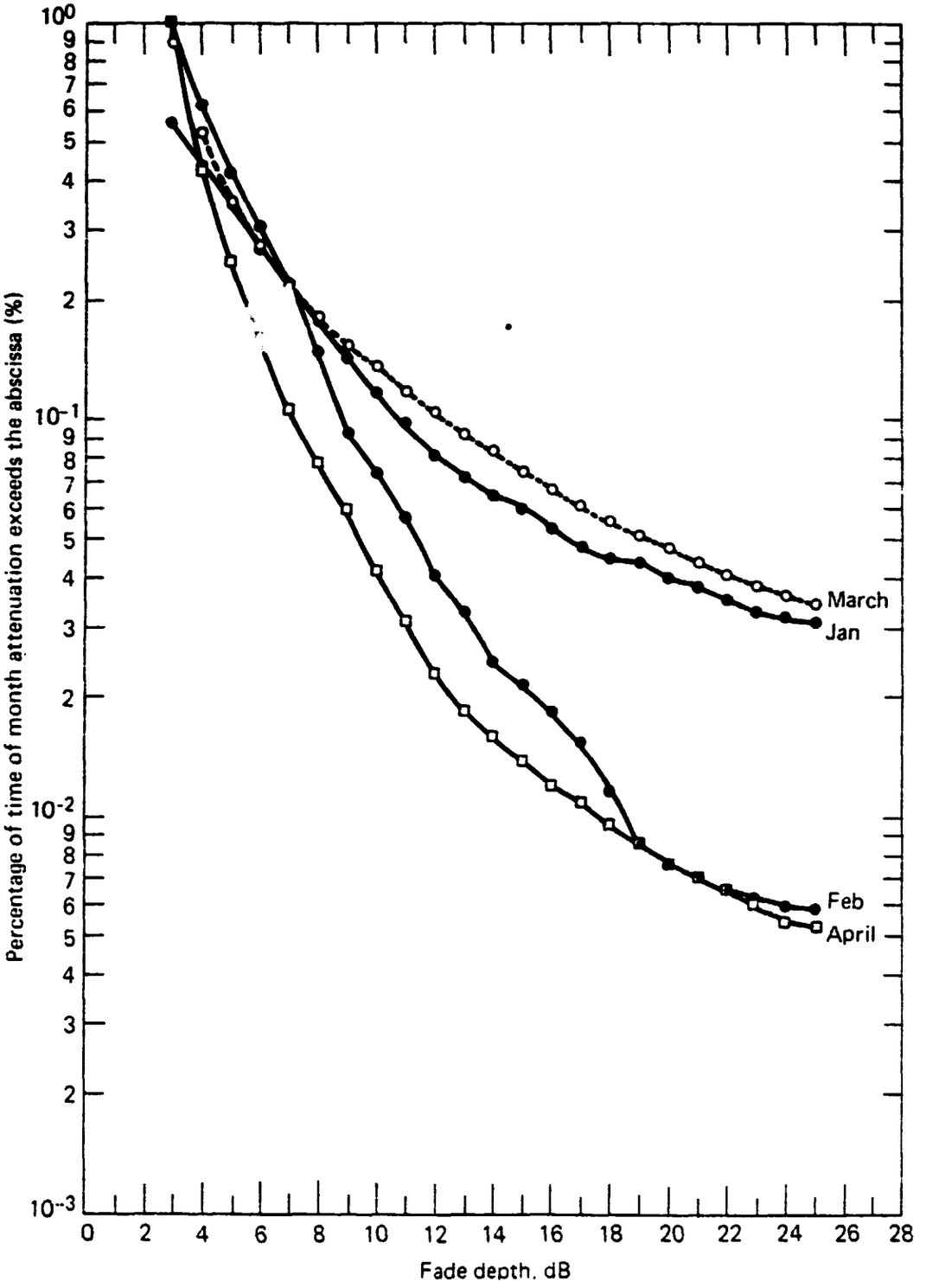


Figure 6. Monthly cumulative fade distributions for combined years (January-April).

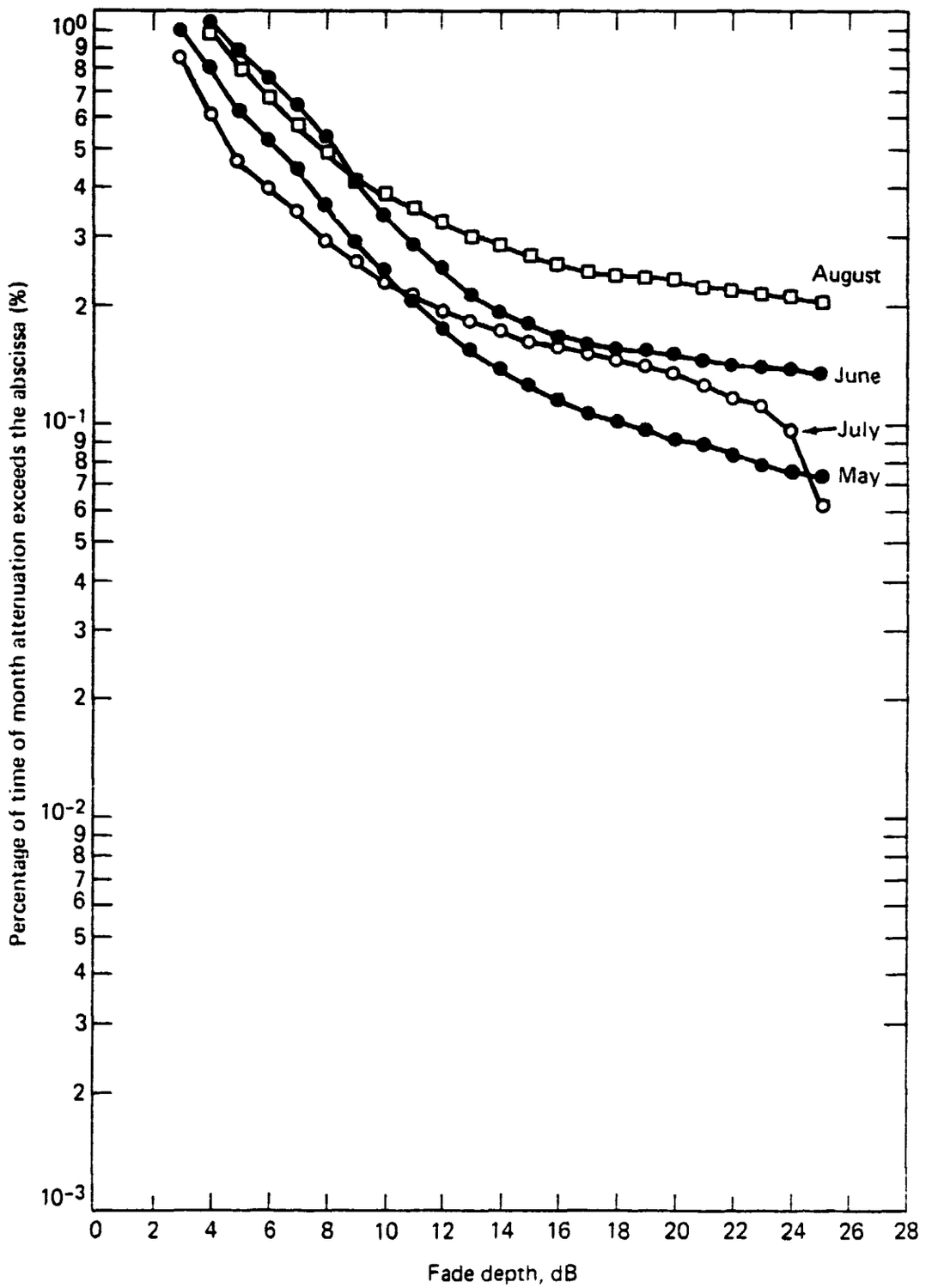


Figure 7. Monthly cumulative fade distributions for combined years (May-August).

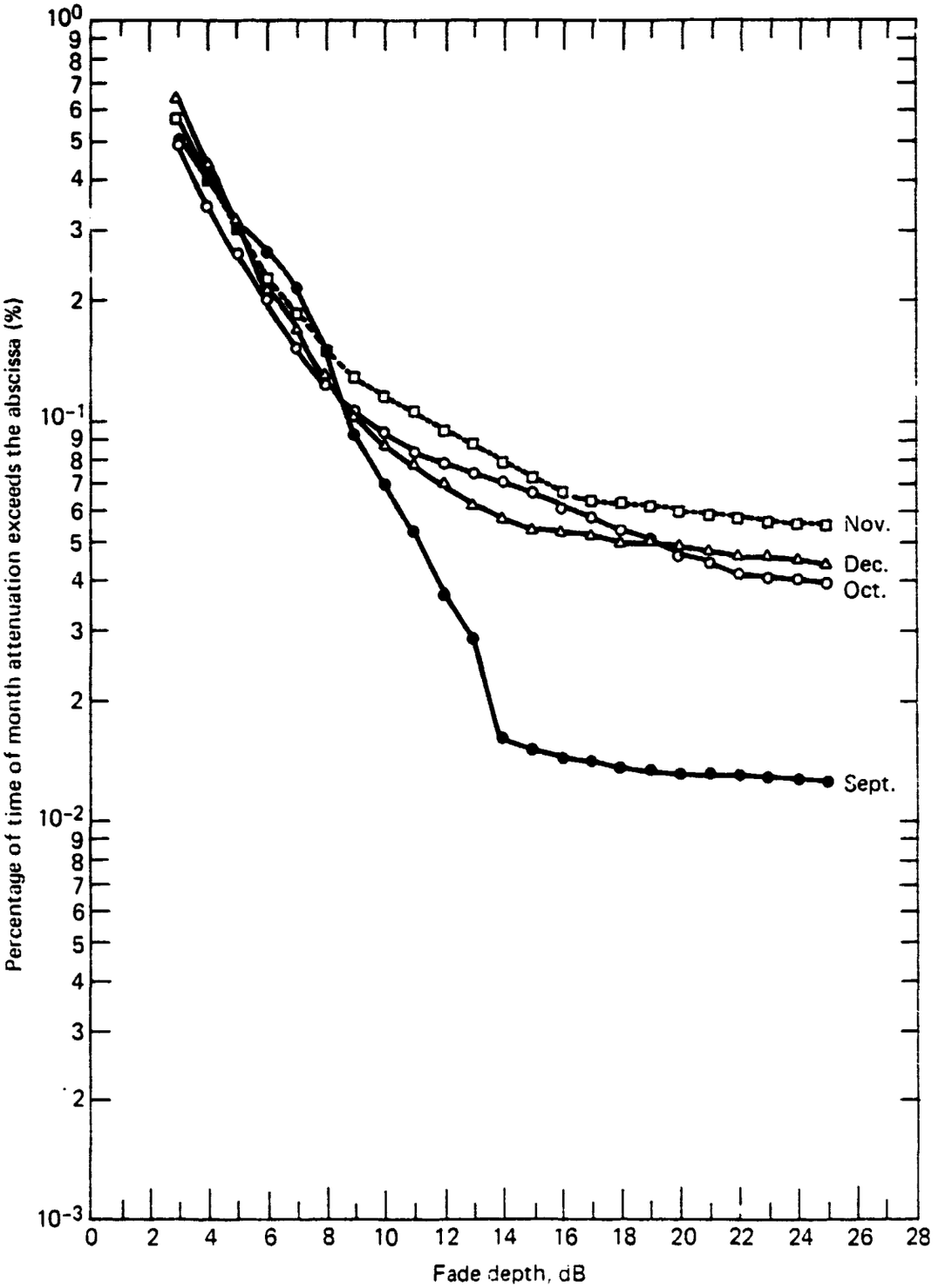


Figure 8. Monthly cumulative fade distributions for combined years (September-December).

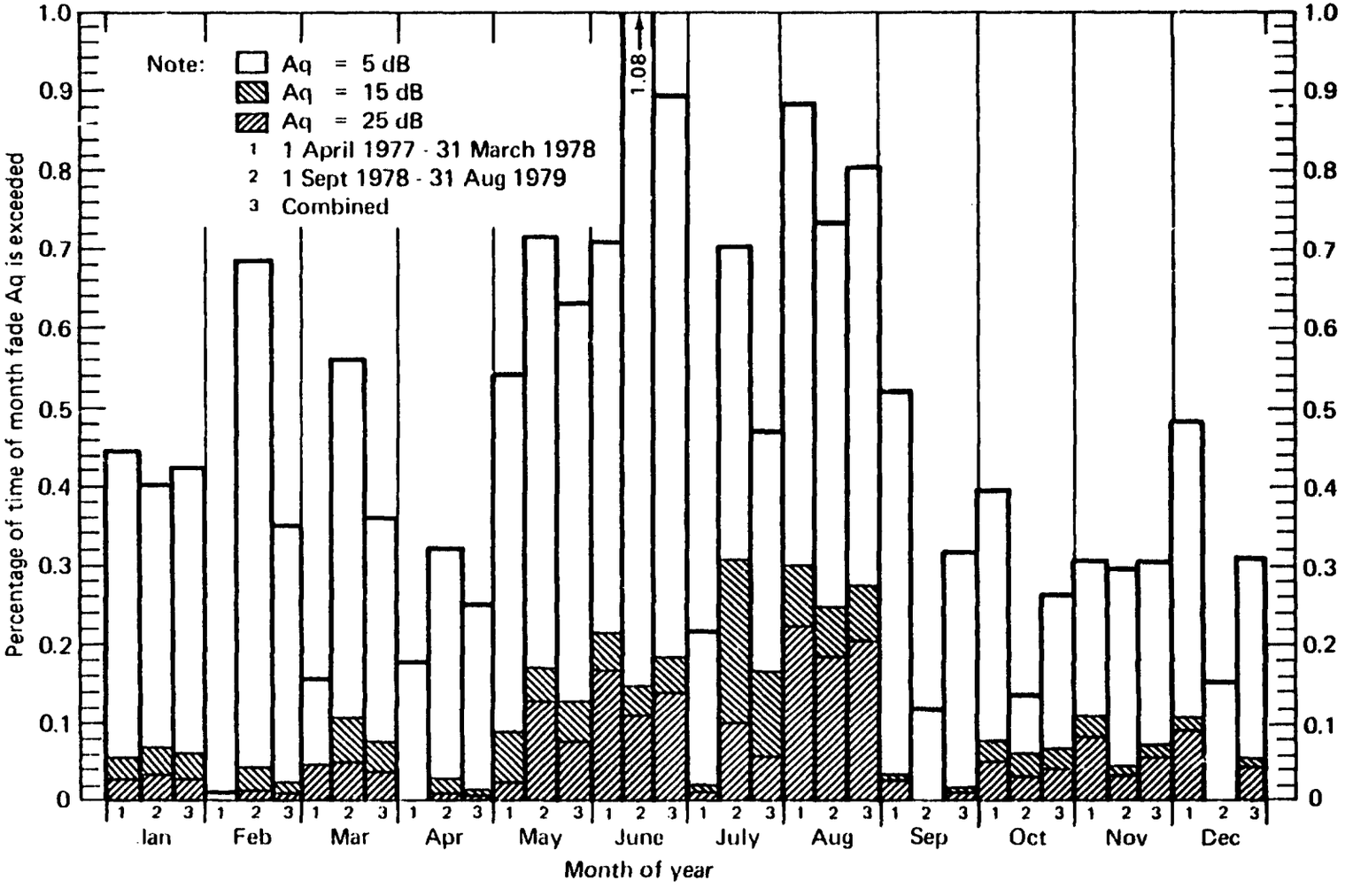


Figure 9. Histogram depicting exceedance times at 5, 15, and 25 dB levels for 1st, 2nd, and combined years data bases as a function of month of year.

We also note that considerable year to year variation exists. Six of the twelve months have exceedance times which differ by more than a factor of 2 when comparing the first and second years at thresholds of 15 dB and greater (February, April, July, September, November, and December).

### 3.5 Time of Day Statistics

In Fig. 10 are given the fade distributions at 28.56 GHz using the combined data base for 6 contiguous time slots of four hours each. The ordinate represents the percentage time of year the abscissa levels of fades are exceeded, where the individual time slots are in GMT; EST at Wallops Island, Virginia being 4 and 5 hours earlier during the summer and winter months, respectively (i.e., the difference being due to daylight saving time). We note that at fades of 12 dB and greater the distributions separate into 3 groupings. The grouping with the highest exceedance times (more than double the other groupings) have 3 contiguous time slots which range from 1600 to 0400 GMT (noon to midnight, EST, for the summer period).

In Fig. 11 is given a histogram depicting the year to year variations of the exceedance times as a function of the time of day. The vertical scale represents the percentage of the year, the attenuation exceeds the threshold level $A_q$ where the indicated nomenclature is the same as in Fig. 9. The six time slots of four hours each (GMT) are given along the horizontal axis.

An overview glance at the histogram also depicts the existence of larger exceedance times during the period 1600 through 0400 at threshold levels of 15 dB and greater for the combined year case.

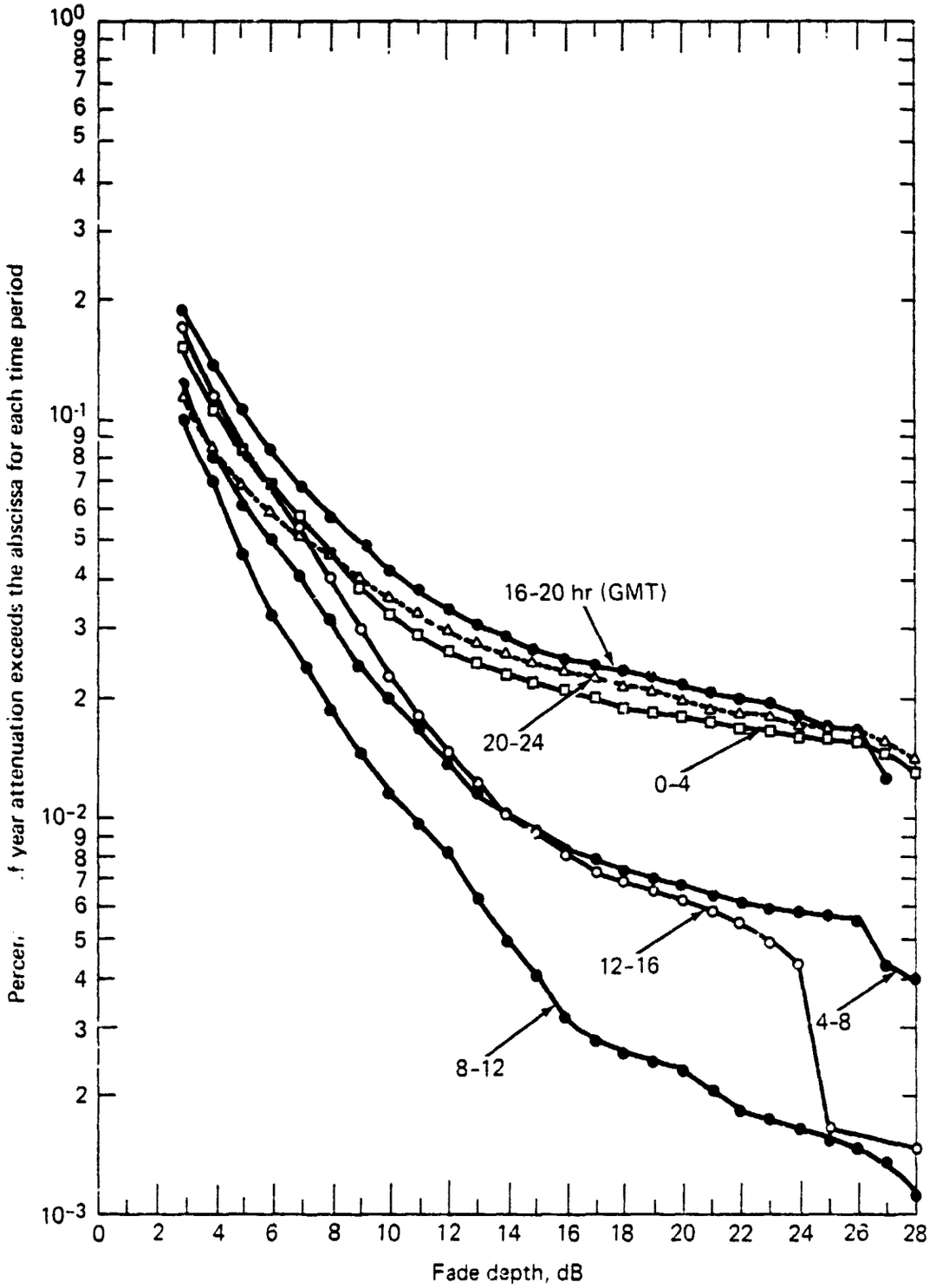


Figure 10. Cumulative fade distributions over combined years period for 6 contiguous time slot intervals (GMT).

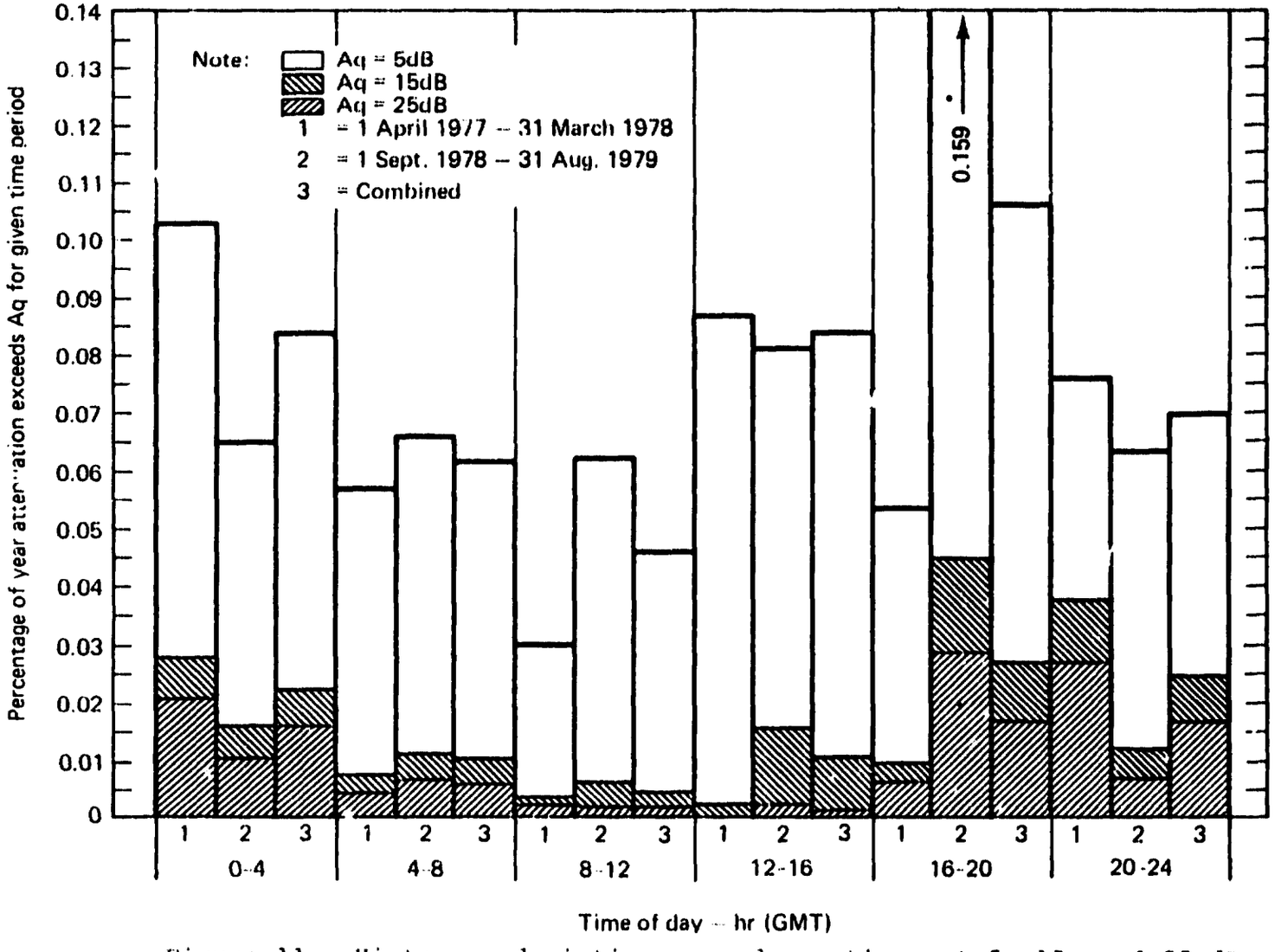


Figure 11. Histogram depicting exceedance times at 5, 15, and 25 dB levels for 1st, 2nd, and combined years data bases as a function of time of day.

Considerable year to year variation is observed at the respective time slots. We note that upon comparing the first and second year, 3 out of the 6 time slots have exceedance times which differ by more than a factor of 2 (12-16, 16-20, and 20-24 hr GMT).

## 4.0 Rain Rate Statistics

In Fig. 12 are given the rain rate distributions measured during the first (triangular data points), the second (circular data points) and combined years (solid points). The combined year's distribution ranges from .75% at 4 mm/hr to .0012% at 140 mm/hr. Beyond 100 mm/hr the data becomes increasingly noisy (exceedance times <.0035% or 18 minutes).

We note that the first and second year's distributions are similar to one another; the second year's exceedance times being slightly larger than the first year's distribution up to a rain rate of 40 mm/hr. At larger rain rates, the curves cross over and the first year's exceedance times are slightly larger. These results are consistent with the yearly fade distributions depicted in Fig. 1; the second year's exceedance times being only slightly larger than those of the first year's up to a fade of approximately 25dB, beyond which the curves cross over.

It is interesting to note from Fig. 13 that the combined year rain rate gives an excellent fit with a log normal distribution down to 100 mm/hr; the rms and peak deviation being less than 4% and 10%, respectively.

In Fig. 14 we examine how the two years of monthly rainfall compare with the average monthly rainfall during a period of 26 to 30 years. Shown in this figure are the average rainfalls (centered horizontal dash) and the respective $\pm$ standard deviations for each of the months (upper and lower horizontal dashes). These curves were deduced from the results supplied by the U.S.

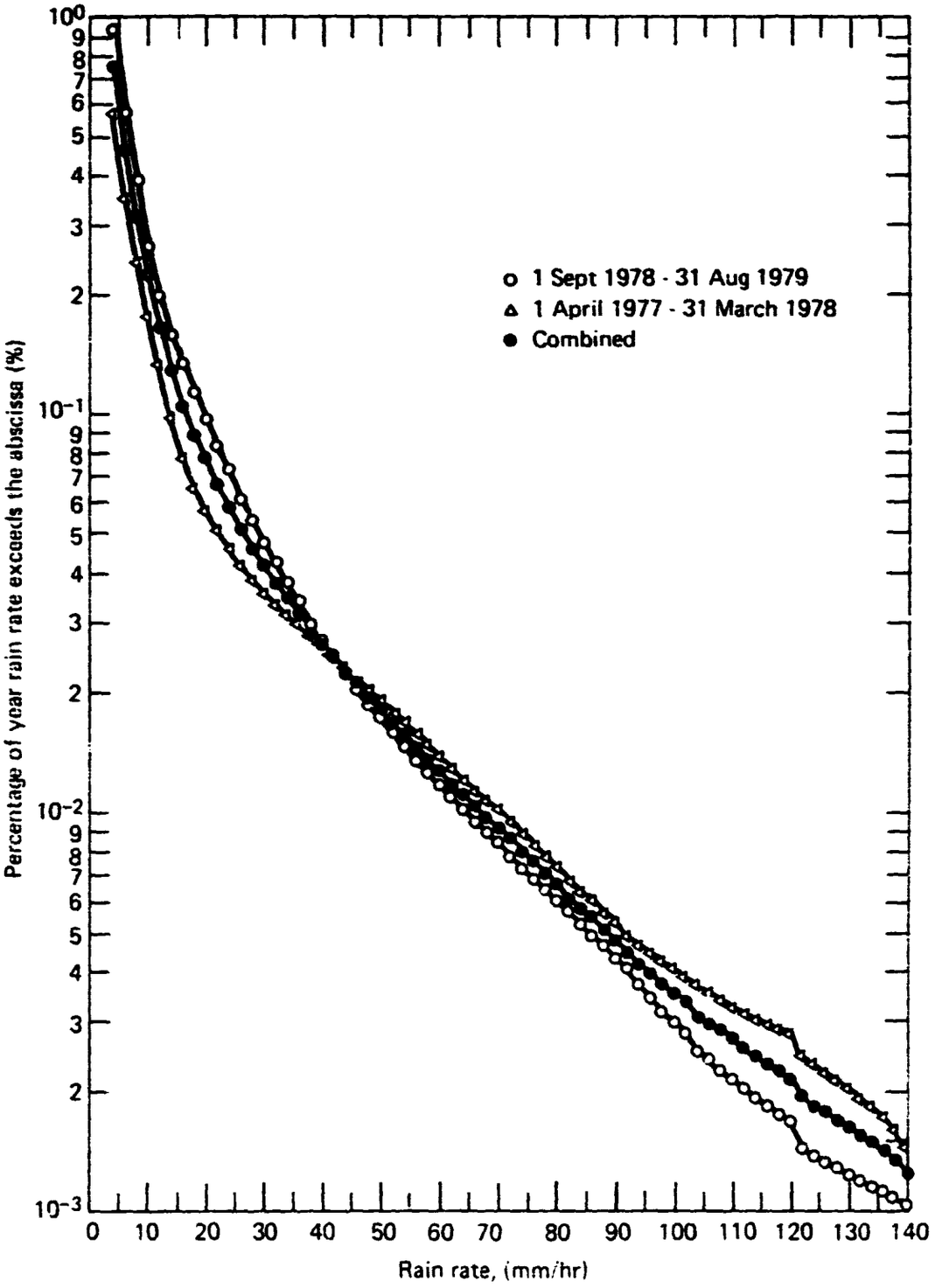


Figure 12. Cumulative rain rate distributions for 1st, 2nd, and combined years data bases.

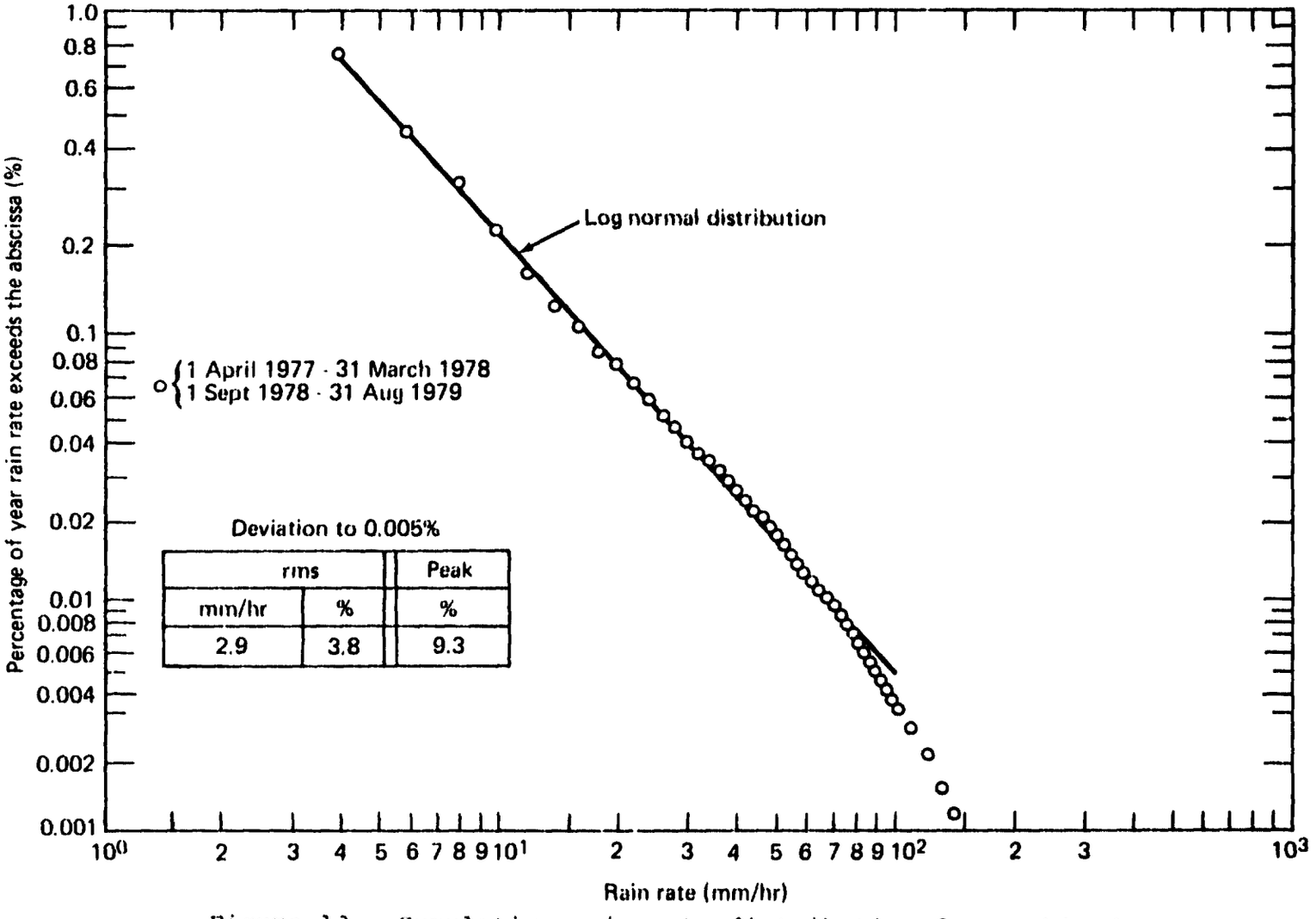


Figure 13. Cumulative rain rate distribution for combined years data base plotted against log-normal scales. The solid curve is fitted down to 100 mm/hr.

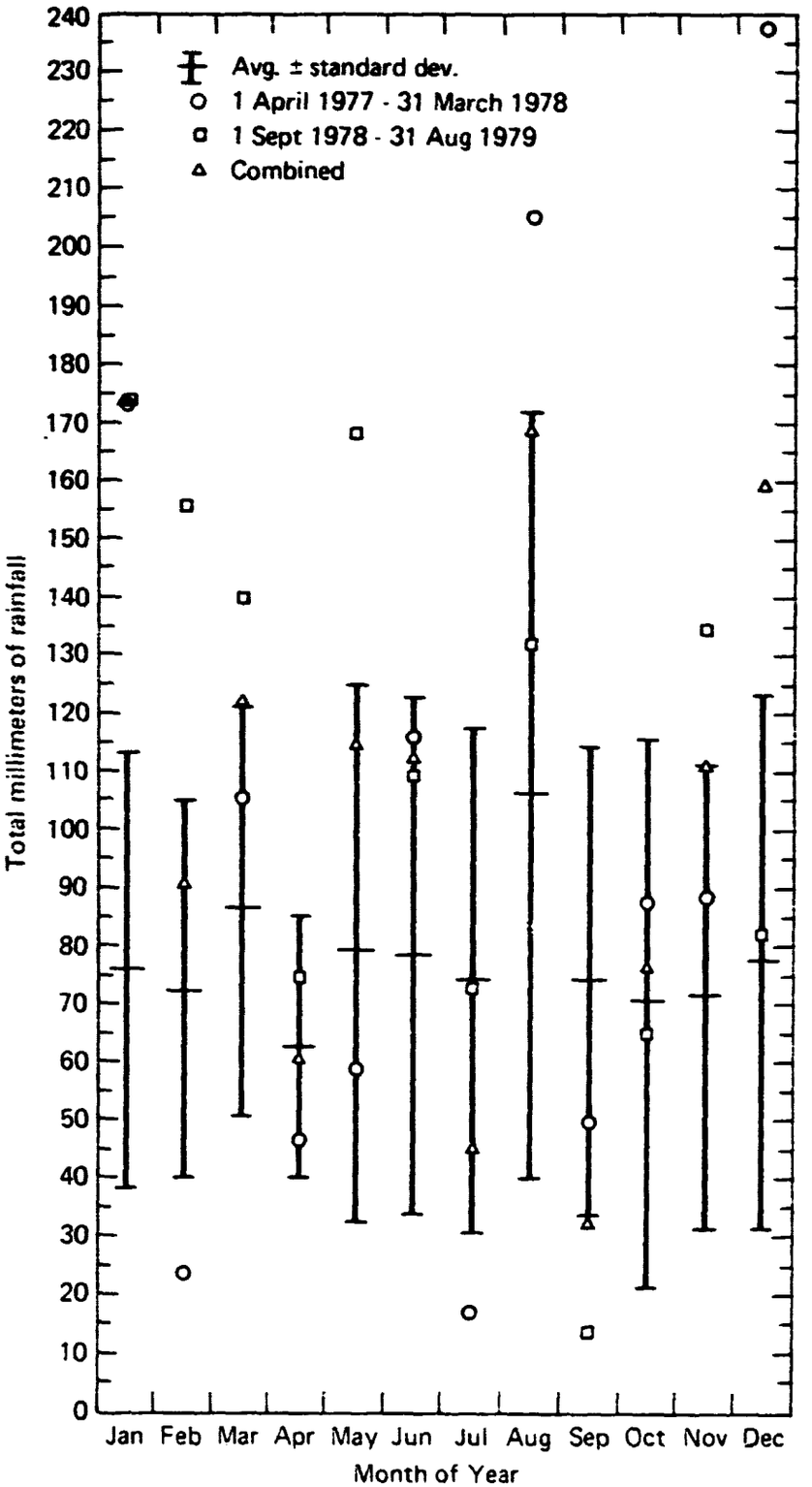


Figure 14. Long term average monthly rainfall with respective ± standard deviations at Wallops Island, Virginia (center dash lines represent the averages and the extreme dash lines denote the ± standard deviations). The data points denote the 1st (circular), 2nd (square) and combined (triangular) monthly rainfall. (Data obtained from the U. S. Navy and U. S. Weather Service for the Wallops Station.)

Navy and U.S. Weather Service for the Wallops Station. Also shown, are the total rainfalls over the first (circular data point) and second year (square data point) as well as the combined years (triangular points). It is interesting to note that August, the "worst" fade month, shows the largest average rainfall as well as the largest standard deviations.

We also observe that when the individual year's rainfall are taken by themselves they are not representative of the long term average monthly rainfall. For example, during the first and second year, the individual rainfalls are outside the vertical lines (depicting the average with the plus and minus standard deviations) 5 out of 12 months, and 6 out of 12 months, respectively. When the two years are, however, averaged together, the combined months rainfall are within or border those of the average month in 10 out of 12 cases (triangular points), thus demonstrating the necessity for acquiring data over a multiyear period.

## 5.0 Prediction of the Fade Distributions at 19.04 GHz

In this section we review and test the formulation for predicting the fade statistics at a second frequency, given a knowledge of the distributions of the fades at a first frequency and of the rain rates.

### 5.1 Effective Parameters

The path attenuation at a frequency, f, at any fixed percentage, P, is assumed given by the relation,

$$A(f) = a\, R^{b}\, \ell_e \quad [dB] \tag{2}$$

where R is the ground measured rain rate (mm/hr) at the percentage, P, $\ell_e$ is the effective path lengths (km) over which a uniform R gives A(f). Also, a and b are empirical parameters which are primarily frequency and drop size distribution dependent. Considering relations of the form (2) at 28.56 and 19.04 GHz and dividing the former attenuation by the latter, we arrive at,

$$\frac{A_{28}}{A_{19}} = \alpha\, R^{-\beta} \tag{3}$$

where,

$$\alpha = \frac{a_{28}}{a_{19}}, \qquad \beta = \beta_{19} - \beta_{28} \tag{4}$$

and where the subscripts denote the defined parameters at the respective frequencies. It is tacitly assumed in the determination of (3), that the effective path length is frequency invariant, at least over the frequency interval of 19 to 28 GHz. They therefore cancel out in the ratio.

In Table 2 are given the calculated parameters, $\alpha$, and $\beta$ employing from the tabulations of Olsen et al (13) for the Marshall-Palmer distribution (14) and Joss distribution for thunderstorm (15). Also given are the calculated parameters derived from the best fit regression relationships derived from drop size spectra, measured at Wallops Island, Virginia,(hereafter referred to as the APL distribution). These data were derived from 5 rain days during the summer of 1977 and 5 rain days during the fall-winter of 1978-79 (17 hours of disdrometer data) (4,16).

We note that the values of $\alpha$ or $\beta$ for the three cases are very similar even though the drop size spectra corresponding to the Joss and Marshall-Palmer distributions are very much different. We also observe from the smallness of the quantity, $\beta$, for all the cases, a minimal dependence on rain rate.

These results are consistent with the notion that the ratio of attenuations at frequencies not too widely displaced are relatively invariant to drop size spectra as theoretically demonstrated by Goldhirsh (3).

Table 2

Empirical parameters deduced from results of Olsen et al (13) for Marshall-Palmer and Joss (thunderstorm) cases and from APL distribution. All calculations were made for T=20°C. The parameters are defined by equations (2), (3) and (4).

| Drop Size Distribution | $a_{28}$ | $a_{19}$ | $b_{28}$ | $b_{19}$ | $\alpha$ | $\beta$ |
|---|---|---|---|---|---|---|
| Marshall-Palmer (14) | 0.171 | .0661 | 1.041 | 1.114 | 2.59 | .073 |
| Joss-Thunderstorm (15) | .244 | .0936 | 0.831 | 0.940 | 2.61 | .109 |
| APL (16) | .1695 | .0710 | 1.018 | 1.063 | 2.39 | .045 |

## 5.2 Testing of the Various Empirical Relations

In Fig. 15 are plotted radar derived fade distributions (solid points) at 28.56 and 19.04 GHz obtained from 17 hours of radar data over the same period that the drop size spectra were measured at Wallops Island, Virginia. These fade distributions were derived by converting radar measured rain reflectivities along the earth-satellite path to partial attenuation contributions and summing to obtain the integrated path attenuations at any instant of time (4, 16).

The ordinate in Fig. 15 represents the percentage of the total observation time (17 hours) in rain that the abscissa values of attenuations are exceeded. The radar derived distributions are given by the solid curves and these are assumed to be the true or test distributions. Confidence in these distributions was established by comparing the 28.56 GHz case with the directly measured beacon distribution over the same time period, resulting in an approximate 1 dB rms deviation (4, 16).

Shown in the vicinity of the solid curves are circled points denoting predicted levels using the form (3). Hence, the circular points for the 19.04 GHz case were obtained using the radar derived fade distribution at 28.56 GHz (solid curve), the measured rain rate distribution (at equal percentages) over the same period (not shown) and the disdrometer derived results in Table 2. Similarly, the circular points at 28.56 GHz were obtained using the radar derived 19.04 GHz fades. The proximity of the predicted and radar derived distributions demonstrate the ability

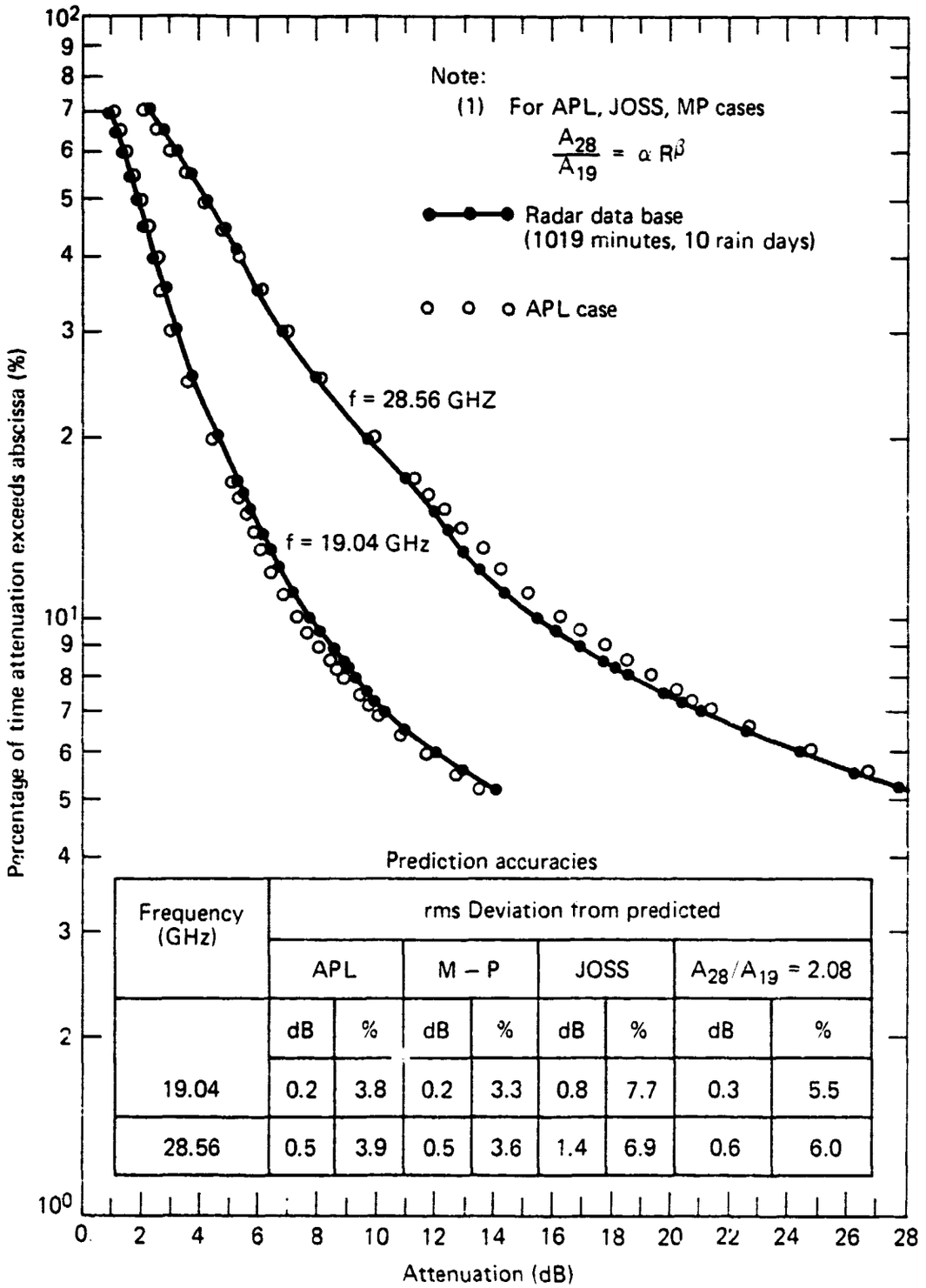


Prediction accuracies

| Frequency (GHz) | rms Deviation from predicted | | | | | | | |
|---|---|---|---|---|---|---|---|---|
| | APL | | M – P | | JOSS | | $A_{28}/A_{19}$ = 2.08 | |
| | dB | % | dB | % | dB | % | dB | % |
| 19.04 | 0.2 | 3.8 | 0.2 | 3.3 | 0.8 | 7.7 | 0.3 | 5.5 |
| 28.56 | 0.5 | 3.9 | 0.5 | 3.6 | 1.4 | 6.9 | 0.6 | 6.0 |

Figure 15. Radar derived conditional fade distributions (solid points) compared with predicted levels (circled points). Radar data covers 17 hours of rainfall during 5 summer and 5 winter rain days.

to predict up or down in frequency. In Fig. 15 is given also a table comparing the various rms deviations for other distributions. We note that the rms deviations for the APL, M-P, and Joss cases are less than 4%, 4%, and 8%, respectively, when comparing the predicted and test distributions at both frequencies.

As previously mentioned, the average ratio of attenuation of the radar derived levels resulted in the factor 2.08 with a standard deviation of 0.13 (Table 1). When this factor is used to either predict up in frequency (28 GHz) using the 19 GHz distribution or down (19 GHz) using the 28 GHz distribution, rms uncertainties of 6% and less are noted (see table in Fig. 15).

We thus note that all of the above predictions give very respectable agreement with the test distributions; demonstrating quantitatively that the ratio of attenuation is relatively invariant to drop size spectra.

Because of the excellent agreement in Fig. 15, the 19.04 GHz fade distribution for the overall data base was derived using the relationship (2) in conjunction with the APL parameters in Table 2, the combined fade distribution at 28.56 GHz (Fig. 2), and the overall rain rate distribution (Fig. 12).

## 6.0 Comparison with Refinement of C.C.I.R. Global Model

In this section we compare the cumulative distributions in Fig. 2 with those predicted using a refinement (17) of the global model developed by Crane (18). The former C.C.I.R. model (19) divided the world up into 5 climatological regions as opposed to 8 regions for the refined case. In the prediction model used (18), the U.S. is divided up into 5 regions; Wallops Island being called region D (Continental). Region D is further subdivided up into 3 subregions ($D_1$, $D_2$, and $D_3$) to better describe the climatic variations. Each region or subregion has associated with it a designated rain rate distributions deduced from available experimental data.

In Fig. 16 are depicted rain rate distributions (smooth curves) for regions $D_3$ (south of Wallops Island) and $D_2$ (region of Wallops Island). The dotted curve represents the measured distribution using the combined two year data base for Wallops Island, Virginia. We note that for rain rates up to 50mm/hr the distribution lies between curves $D_2$ and $D_3$. At higher values, the Wallops distribution exceeds those of $D_3$. According to the global mode, a fade at 28.56 GHz of 27 dB (approximate upper value measured at Wallops Island) corresponds to an effective rain rate of 23mm/hr (.045%). As noted in Fig. 16, relatively close agreement exists between the global model and the measured distribution of rain rates up to this upper value of 23mm/hr.

In Fig. 17 are given the comparisons of the global model fade distributions with those obtained for Wallops Island, Virginia.

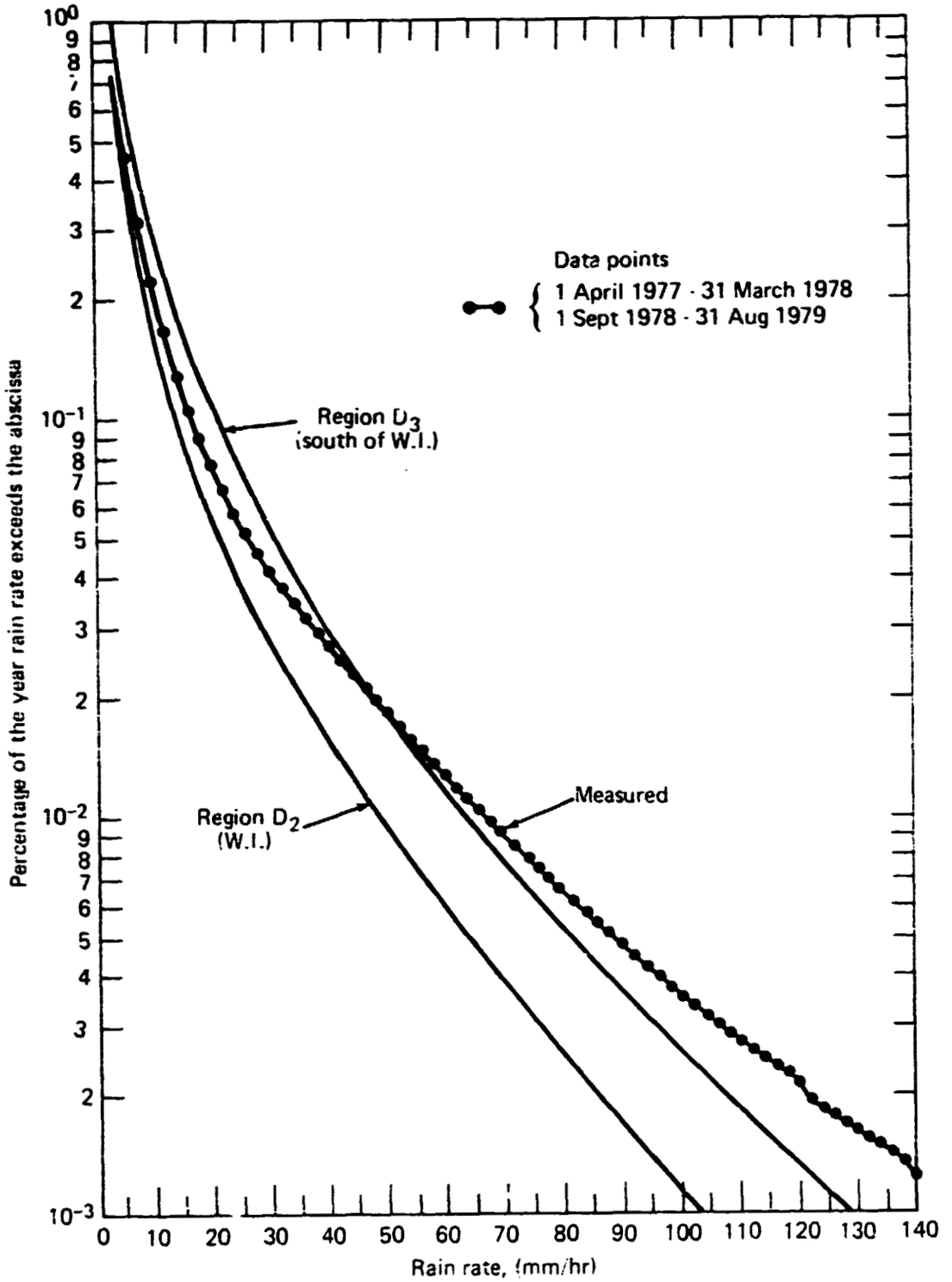


Figure 16. Rain rate distributions for Regions $D_2$ and $D_3$ of global model (18) compared with measured distributions (combined years) for Wallops Island, Virginia

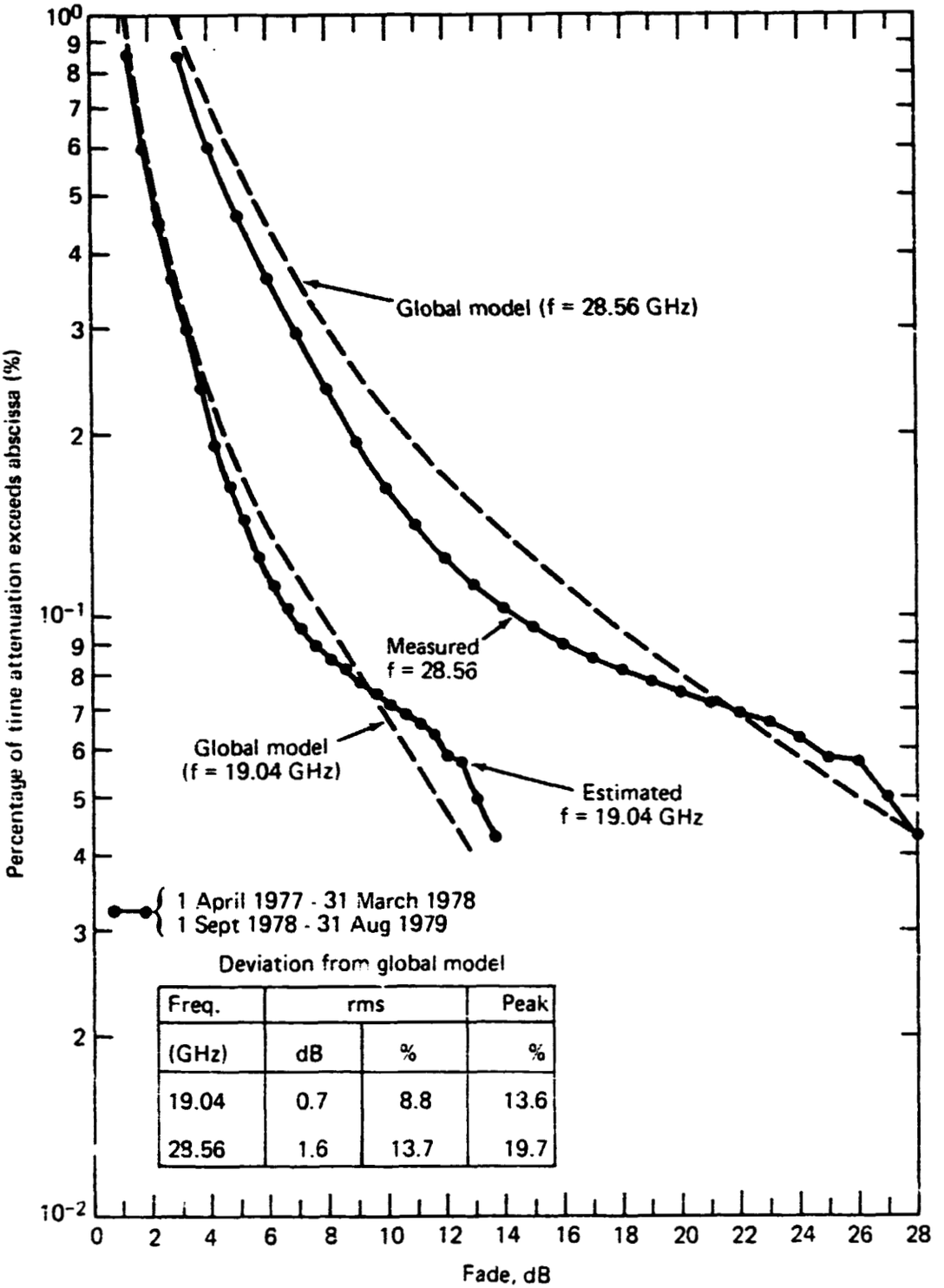


Figure 17. Comparison of cumulative fade distributions for Wallops Island, Virginia, with those predicted using the global model (18).

We note that agreement is relatively good; the peak deviations over the fade range shown are less than 20% and 14% for 28.56 and 19.04 GHz, respectively, and the rms deviations are less than 9% and 14%. In calculating the predicted curves, the model rain rate for region $D_2$ was used (18).

## 7.0 Summary and Conclusions

Multiyear rain fade statistics at 28.56 GHz and 19.04 GHz are presented here for the climatological region of Wallops Island, Virginia. These results are important for designers of earth-satellite communication's systems who require reliable fade statistics for establishing link-margin requirements. Reliable statistics may be compiled only through the examination of multiyear data bases. For example, Crane (1) showed that at least two or more years are generally required to achieve a meaningful fade distribution down to .01% of the time with a reasonably small standard error (less than 10%).

In this work, fade statistics are given which provide the communicator with yearly cumulative fade distributions as well as "time of day" and "month of year" fade statistics. This latter information is useful for ascertaining diurnal and monthly power demands for systems employing variable transmitter power capabilities.

The salient results of this work are as follows:

1) The fade distribution characteristics show that exceedance times of approximately 1% to .04% correspond to fades between 3 and 26 dB, respectively. At 19.04 GHz, the corresponding fades range from 1.3 to 12.6 dB (Fig. 2).
2) Although the monthly and time of day distributions possess considerable year to year variability, the overall fade distributions for the individual years

are similar to one another. For example, the second year's fades are within an 18% rms deviation of those for the first year (Fig. 1). Whether this is fortuitous or not will be established by examining future data bases.

3) The average ratio of fades calculated from the 28.56 and 19.04 GHz combined years distributions at equal time percentages was found to be 2.12 with a standard deviation of 0.05. This ratio is close to those derived from similar type fade statistics obtained at other locations (Table 1) supporting the relative invariance of this ratio with drop size distribution.

4) The cumulative distributions at 28.56 and 19.04 GHz follow with good approximation log normal distributions (the rms deviation being less than 7% for exceedance times down to .05%; Fig. 5). The rain rate distribution also follows with good approximation a log normal distribution down to 0.005% of the time (e.g., the rms deviation is less than 4%; Fig. 13).

5) August was found to be the "worst month" (maximum exceedance times) at the extreme fade of 25dB for both years (Fig. 9) and for all fades exceeding 10dB for the combined years (Fig. 7).

6) May through August (combined years) have exceedance times which are more than double those of the other 8 months for fades of 15dB and greater (Figs. 6-8).

7). Considerable year to year variability exist for both the "monthly" and "time of day" statistics. For example, 6 of the 12 months have exceedance times which differ by more than a factor of 2 when comparing the first and second years at 15dB thresholds and greater (Fig. 9). In addition 3 out of the 6 time slots (4 hours each) have exceedance times (at 15 dB thresholds and greater) which likewise differ by more than a factor of 2 when comparing the individual years (Fig. 11).

8). Exceedance times were greatest at fades of 12dB and more in the time slots from 1600 to 0400 GMT (noon to midnight during the summer). In fact, they are more than double those exceedance times pertaining to other times of the day (Fig. 10).

9). The rain rate distribution depicts a rate of 4 to 140 mm/hr over 0.75% to 0.0012% exceedance time, respectively. Beyond 100mm/hr, the data appears increasingly noisy (Fig. 12).

10). Using effective path length concepts (equation (13)), the fade distribution has been demonstrated to be predictable to within 4% (rms) of the radar derived fade distributions at 19.04 and 28.56 GHz (Fig. 15). This proximity supports the usefulness of this procedure for predicting fade distributions at other frequencies.

11). The ratio of fades at 28.56 and 19.04 GHz has been quantitatively demonstrated to be relatively invariant to drop size distribution. A theoretical argument demonstrating this characteristic has been previously given (3).

12). The fade distributions at 28.56 and 19.04 GHz give rms fade deviations which were within 14% and 9%, respectively, from those derived using a global prediction model (18) which represents a refinement of a previous model (17).

## 8.0 References

(1) Crane, R. K., "Prediction of the Effects of Rain on Satellite Communication Systems", Proc. IEEE, Vol. 65, pp. 456-474, 1977.

(2) Cox, D. C., "An Overview of the Bell Laboratories 19 and 28 GHz COMSTAR Beacon Propagation Experiments", Bell Syst. Tech. J., Vol. 57, No. 5, pp. 1231-1255, 1978.

(3) Goldhirsh, J., "Cumulative Slant Path Rain Attenuation Statistics Associated with the COMSTAR Beacon at 28.56 GHz for Wallops Island, Virginia", IEEE. Trans. Antennas and Propagation, Vol. AP-27, No. 6, November 1979.

(4) Goldhirsh, J., "Predictive Methods for Rain Attenuation Using Radar and In Situ Measurements Tested Against the 28 GHz COMSTAR Beacon Signal", IEEE Trans. Antennas and Propagation, Vol. AP-27, No. 3, pp. 398-406, May 1979.

(5) Cox, D. C., H. W. Arnold, and H. H. Hoffman, "Depolarization of 19 and 28 GHz Earth-Space Signals by Ice Particles", Radio Science, Vol. 13, No. 3, pp. 511-517, May-June 1978.

(6) Rowland, J. R., "Comparison of Two Different Raindrop Diameters", Proc. 17th Radar Meteorology Conf., Seattle, Washington, AMS, pp. 398-405, 26-29 October 1976.

(7) Gebo, H., "Description of the Disdrometer Data FIFO Register", APL/JHU Technical Memorandum, S1R79U-030, November 1979.

(8) Drufuca, G., "Rain Attenuation Statistics for Frequencies above 10 GHz from Radar Observations", J. De Recherches Atmospheriques, Colloque De L'IUCRM, Vol. VIII, pp. 413-420, Jan.-June 1974.

(9) Harris, J.M. and G. Hyde, "Preliminary Results of COMSTAR 19/28 - GHz Beacon Measurements at Clarksburg, Maryland", COMSAT Tech. Rev., Vol. 7, No. 2, pp. 599-624, Fall 1977.

(10) Bergmann, H. J., "A MM Wave Propagation Experiment in Georgia and Illinois Utilizing COMSTAR Beacon Signals", 1978 International IEEE/AP-s Symposium, USNS/URSI Spring Meeting, Washington, D. C., 15-19 May 1978.

(11) Cox, D. C., H. W. Arnold and A. J. Rustako, Jr., "Attenuation and Depolarization by Rain and Ice Along Inclined Radio Paths through the Atmosphere at Frequencies Above 10 GHz", EASCON 79 Conference Reccrd 79CH1476-1 AES, Vol. 1, October 9-11, 1979, Sheraton National Hotel, Arlington, Virginia, pp. 56-61.

(12) Lin, S. H., "Statistical Behavior of Rain Attenuation", The Bell System Tech. J., Vol. 52, No. 4, pp. 557-581, April 1973.

(13) Olsen, R. L., Rogers, D. V. and D. B. Hodge, "The $aR^b$ Relation in the Calculation of Rain Attenuation", IEEE Trans. Antennas Propagation, Vol. AP-26, pp. 318-320, March 1978.

(14) Marshall, J. S. and Palmer, W. McK., "The Distribution of Raindrops with Size", J. Meteorol., Vol 5, pp. 165-166, 1948.

(15) Joss, J., Thams, J. C., and Waldvogel, A., "The Variation of Raindrop Size Distribution in Locarno", in Proc. Int. Conf. on Cloud Physics, Toronto, Ont., Canada, Aug. 26-30, 1968.

(16) Goldhirsh, J., "Comparison of Radar Derived Rain Attenuation with the COMSTAR Beacon at 28.56 GHz for Summer and Winter Periods", APL Technical Report S1R79U-061, Applied Physics Laboratory/The Johns Hopkins University, Laurel Maryland, July 1979.

(17) Crane, R. K., "A Global Model for Rain Attenuation Prediction", EASCON 78 Record, IEEE No. 78CH1352-4, pp. 391-395, 1978.

(18) Crane, R. K., and Blood, D. W., "Handbook for the Estimation of Microwave Propagation Effects - Link Calculations for Earth-Space Paths", ERT Technical Report No. 1, Document No. P-7376-TR1, Contract No. NAS 5-25341, June 1979 (Environmental Research and Technology Inc., Concord, Mass.).

(19) C.C.I.R. (International Radio Consultative Committee) Recommendations and Reports of the C.C.I.R., 1978, XIVth Plenary Assembly, Kyoto, Vol. V, Propagation in Non-Ionized Media, pp. 82-84. (International Telecommunication Union, Geneva, Switzerland).